

Bismuth Oxychloride Nanowires for Photocatalytic Decomposition of Organic Dyes

Xiangbiao Liao,^{||} Xin Lan,^{||} Nan Ni,^{||} Pengfei Yang, Yuan Yang,* and Xi Chen*Cite This: *ACS Appl. Nano Mater.* 2021, 4, 3887–3892

Read Online

ACCESS |



Metrics & More



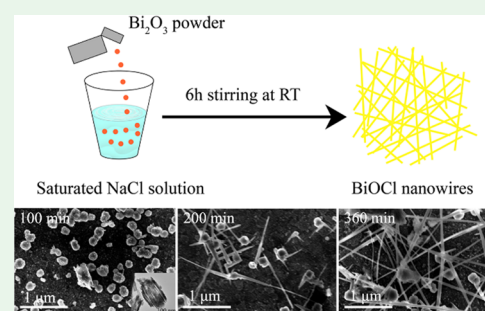
Article Recommendations



Supporting Information

ABSTRACT: Engineering nanostructures for semiconductor materials is recognized as an important strategy for achieving excellent photocatalytic activity. Although multiple nanostructures of bismuth oxychloride (BiOCl) were reported, their synthesis procedures were still complicated and thus limited scalable and practical photocatalytic decomposition. Here, we propose a highly efficient route to achieve BiOCl nanowires through simply stirring the precursor of Bi₂O₃ powder in the saturated NaCl solution at room temperature. The concentration of NaCl plays a crucial role in growing BiOCl nanowires under the mechanism of oriented attachment, uncovered by continuous observations of product morphologies at different reaction stages. Compared to conventional BiOCl powder, BiOCl nanowires exhibited favorable energy band structures with narrow band gaps, which are predominated by the unique structure with a high aspect ratio and exposed active {001} facets. A superior visible-light photocatalytic activity for degrading Rhodamine B dye was found in the case of the prepared BiOCl, which is faster than that for BiOCl nanoparticles and TiO₂.

KEYWORDS: bismuth oxide, bismuth oxychloride, nanowire, crystal growth, photocatalytic degradation



1. INTRODUCTION

Semiconductor-based photocatalysis has become a rapidly growing research area due to its promising applications in environmental pollution remediation and selective energy conversion.^{1–4} Electron–hole pairs can be excited in photocatalytic materials by photons with energy higher than their band gap; however, only UV light can be utilized by conventional TiO₂ due to its wide band gap.⁵ In addition to strategies of photosensitization and heterogeneous semiconductors, more efforts have been paid to exploit novel photocatalysts working under visible light, such as carbon nitride *g*-C₃N₄, metal–organic framework compounds, and graphene-based photocatalysts.^{6–9} The excellent photocatalytic performance of bismuth oxychloride (BiOCl), characterized as a class of quasi-two-dimensional ternary oxide semiconductors composed of [Bi₂O₂] slabs interleaved with two chloride atoms, has attracted intensive industrial and research attention.^{2,10} The open crystalline structure and the intrinsic property of rich oxygen vacancies are favorable for improving its charge transport and separation efficiency of photo-induced electron–hole pairs.¹¹ These unique properties lead to promising potential applications in wastewater purification, water splitting, and selective oxidation of organics.^{12–15} Two main technologies of hydrolysis and solvothermal methods have been widely adopted to prepare BiOCl powder samples using the raw material of BiCl₃. Compared to TiO₂, synthesized BiOCl materials exhibit not only chemically

inert, nontoxic, and costly effective characteristics but also more stable photocatalytic activity.^{11,16}

In addition to doping and defect engineering, advanced designs in BiOCl nanostructures further motivate the rapid development in the photocatalysis field.^{17,18} The BiOCl nanostructures, including nanosheets/nanoplates,^{12,19} hierarchical nanoflowers,²⁰ and hollow microspheres,^{20,21} exhibit superior advantages of high specific surface area, large fraction of exposed active facets, and variation of electronic structures. Moreover, one-dimensional (1D) nanostructures with a high aspect ratio can facilitate the fast separation of electron–hole pairs and favor high photocatalytic reactivity for BiOCl semiconductors.^{22,23} However, the nature of the quasi-two-dimensional structure in the BiOCl crystal challenges the formation of 1D nanowires/nanofibers, which is unfavorable under thermal or chemical treatment.²⁴ Synthesis strategies of electrospinning, the Bi₂O₃ nanowire templates, and the anodic aluminum oxide template via the sol–gel method are recently reported to grow BiOCl nanowires for efficient photocatalytic degradation of contaminants.^{2,11,22,23} However, such methods

Received: January 29, 2021

Accepted: March 31, 2021

Published: April 13, 2021



are not scalable for practical applications and the growth mechanisms of BiOCl nanowires still remain elusive.

Herein, we develop an extremely simple strategy to synthesize BiOCl nanowires in mass production through stirring Bi₂O₃ powder in the saturated NaCl solution at room temperature (Figure 1a). The proposed one-step fabrication

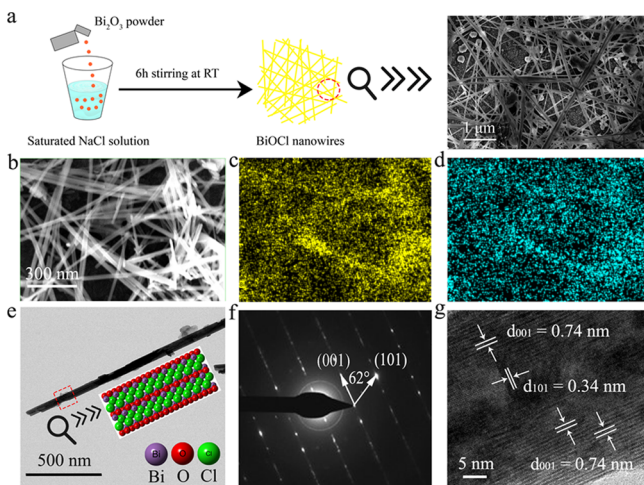


Figure 1. (a) Schematic steps for synthesizing BiOCl nanowires and its SEM image. (b–d) SEM and EDS mapping of Bi and Cl elements of BiOCl nanowires. (e–g) TEM, SEAD pattern, and HRTEM image of the BiOCl nanowire, and the schematic representation of the crystal orientation for nanowires is presented in the inset.

method, taking advantages of mild conditions and non-catalysts/templates involved, is of great significance for enriching techniques of growing semiconductor nanowires (vapor phase growth, templated growth, and solution-based growth methods^{25,26}). The formation mechanism of BiOCl nanowires was well-elucidated through tracing its time-dependent morphologies. Such BiOCl nanowires with a lower band gap exhibited significantly promoted photocatalytic activity compared with commercial BiOCl and TiO₂ through decomposing Rhodamine B (RhB) dye under visible-light irradiation.

2. RESULTS AND DISCUSSION

2.1. Structural Characterization of BiOCl Nanowires.

The product was prepared through stirring Bi₂O₃ powders in the saturated NaCl solution for 6 h (Figure 1a), and the majority of the as-prepared samples is demonstrated to be a network of nanowires. The SEM images (Figure 1a,b) show that the as-prepared nanowires have a high aspect ratio of 50–100 with a length of 2.5–5 μm and diameter of 50 nm. Bi and Cl elements are uniformly distributed in those nanowires as depicted in the EDS images (Figure 1b–d). The TEM image for a single nanowire confirms the size (Figure 1e), and the corresponding selected-area electron diffraction (SAED) pattern displays a spot pattern, demonstrating a single-crystalline nature for the BiOCl nanowires (Figure 1f). The angle of adjacent spots labeled in the SAED pattern is 62°, which corresponds to the theoretical angle between the (101) and (001) planes in BiOCl nanowires.^{2,24} The high-resolution TEM image reveals the lattice fringes for the BiOCl nanowire with interplanar lattice spacings of 0.34 and 0.74 nm, which match well with the (101) and (001) crystalline plane separately (Figure 1g).²⁷ The crystallographic results reveal that the majority of the exposed surfaces around nanowires are {001} facets. It is evident that the as-prepared nanowire is composed of BiOCl with (001)-oriented nanoflakes stacked in the radial direction and grown in its perpendicular direction. We present the modeling crystal representation in the inset of Figure 1e, which demonstrates the nanowire with {001} facets exposed.

We performed X-ray photoelectron spectroscopy (XPS) studies to examine the chemical composition and oxidation state of BiOCl nanowires. Figure S1 shows the peaks of Bi, O, C, and Cl elements in the full scan spectrum, and the presence of carbon contamination signal originates from hydrocarbons in the XPS instrument. The Bi 4f core level spectrum shows two well-resolved peaks located at 158.2 and 163.7 eV, which belong to Bi 4f_{7/2} and Bi 4f_{5/2} of Bi³⁺, respectively. A sharp peak at 529.7 eV corresponding to O²⁻ is confirmed, and two well-resolved peaks are located at 197.1 and 198.7 eV in line with Cl 2p_{3/2} and Cl 2p_{1/2} of Cl⁻.²⁸ Furthermore, using the nitrogen adsorption–desorption method, the specific surface

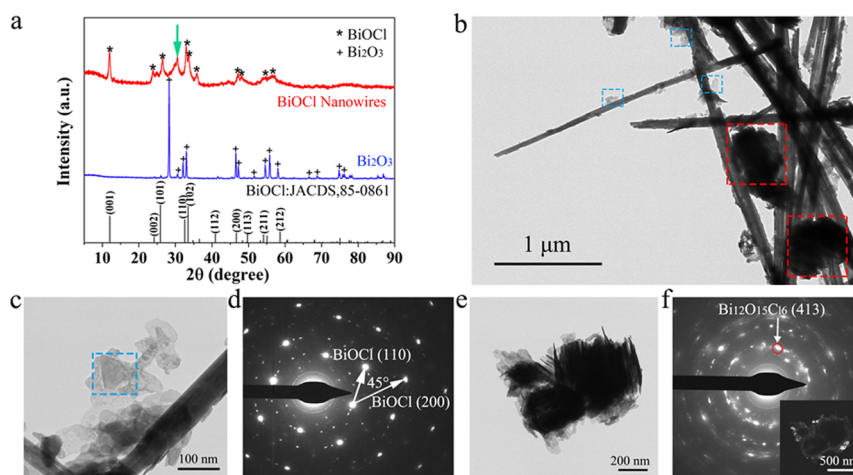


Figure 2. (a) XRD patterns for synthesized BiOCl nanowires and the reactant of Bi₂O₃. (b) TEM image of the coexisting BiOCl nanowires and impure phases in the well-reacted sample; blue and red dashed squares refer to nanoflakes and irregular nanoclusters, respectively. (c) Magnified TEM image of nanoflakes near the BiOCl nanowire. (d) SEAD pattern of nanoflakes inside the blue dashed square. (e) Magnified TEM image and (f) diffraction pattern of irregular nanoclusters.

area of the as-synthesized BiOCl nanowires was measured to be 19.152 m²/g (Figure S2). The value is roughly 100 times larger than that of commercial BiOCl (0.2 m²/g) and twice of that for reported BiOCl nanodisks.²⁴ Due to highly reactive vacancy sites on exposed {001} facets, the large surface area in BiOCl nanowires is favorable for efficient solar-driven photocatalysis.^{19,24,29}

The phase purity and crystallinity of the prepared BiOCl nanowires were confirmed by XRD analysis, and Figure 2a shows the typical XRD patterns for as-synthesized BiOCl and the reactant of Bi₂O₃. The intense and sharp peaks for BiOCl demonstrate that the as-synthesized products are well-crystallized, since the majority of diffraction peaks could be indexed to the tetragonal phase of BiOCl (JCPDS card no. 85–0861). However, the peak at 30.4° marked by the green arrow does not correspond to either the phase of BiOCl or Bi₂O₃, and it is possibly attributed to a certain impure phase. Further investigations were conducted to elucidate the impure phase with obtained structures.

Interestingly, the coexistence of thin nanoflakes (blue dashed squares), irregular nanoclusters (red dashed squares), and well-assembled nanowires was observed in the TEM image of the well-reacted specimen (Figure 2b, Figure S3). Nanoflakes, with a comparable size to the diameter of nanowires, closely attach to the nanowire surface, which suggests the role of nanoflakes as the primary particles for assembling into BiOCl nanowires (Figure 2c). The corresponding SEAD pattern of nanoflakes displays an interplanar lattice spacing of 0.272 nm and an angle of adjacent spots of 45°, indicating a (001) orientation BiOCl crystal for nanoflakes (Figure 2d).¹⁹ Furthermore, we observe a layered structure in irregular nanoclusters consisting of nanoflakes and multiple nanoneedles. In addition to BiOCl crystal spots as depicted in Figure 2f, the marked spot in the diffraction pattern is found to correspond to an interplanar lattice spacing of 0.297 nm and match well with the (413) atomic planes of Bi₁₂O₁₅Cl₆ and the peak of 30.4° in the above-mentioned XRD result.²⁸ Through the technique of dark field STEM, we further find that the Bi₁₂O₁₅Cl₆ phase locates at the edge of such irregular clusters and is brightly illustrated in the inset of Figure 2f. These composite particles are possibly assembled from nanoflakes and further serve as the intermediate basis for the nanowire growth. Thus, the as-synthesized nanowire samples are composed of preassembled BiOCl nanoflakes, intermediate clusters of BiOCl and Bi₁₂O₁₅Cl₆ nanoflakes, and well-assembled BiOCl nanowires. According to the recent study of Bi₁₂O₁₅Cl₆ nanoflakes, such impurities are also favorable for photocatalytic degradation of organics.²⁸

2.2. Growth Mechanism of BiOCl Nanowires. Multiple coexisting phases mentioned above suggest that the oriented attachment (OA) growth mechanism dominates BiOCl nanowire growth with nanoflakes as the primary particle and nanoclusters as the intermediate phase.^{30,31} The morphologies of nanowires at different reaction stages were continuously traced. At the early stage, Cl⁻ reacts with Bi₂O₃ via the reaction: Bi₂O₃ + 2NaCl + H₂O → 2BiOCl + 2NaOH, and BiOCl nanoflakes are formed or Bi₂O₃ particles directly transit into BiOCl nanoclusters. At a time of 100 min, we observe multiple nanoneedles protruding outward the nanoclusters with layered structures and a serrated surface (Figure 3a). It is likely to result from the coalescence of formed primary nanoflakes on the (001) planes and the preferred alignment along the perpendicular direction. The preferred assembly is

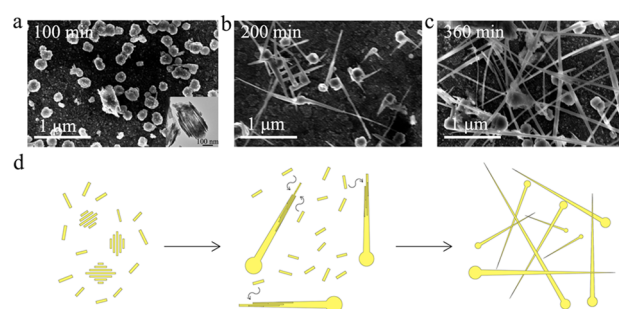


Figure 3. SEM morphologies of BiOCl products from the reaction of Bi₂O₃ in the saturated NaCl solution with the stirring time of (a) 100 min, (b) 200 min, and (c) 360 min. (d) Schematic mechanism for nanowire growth at different reaction stages.

also confirmed by more evidence of the stepped structures and nanotips attached to nanoclusters (Figure S3). As a comparison, the classic crystallization tends to form a 3D bulk microstructure. Nanoneedles keep growing and evolve into a longer nanowire structure at the stage of 200 min (Figure 4b). The formation of longer nanowires may deplete

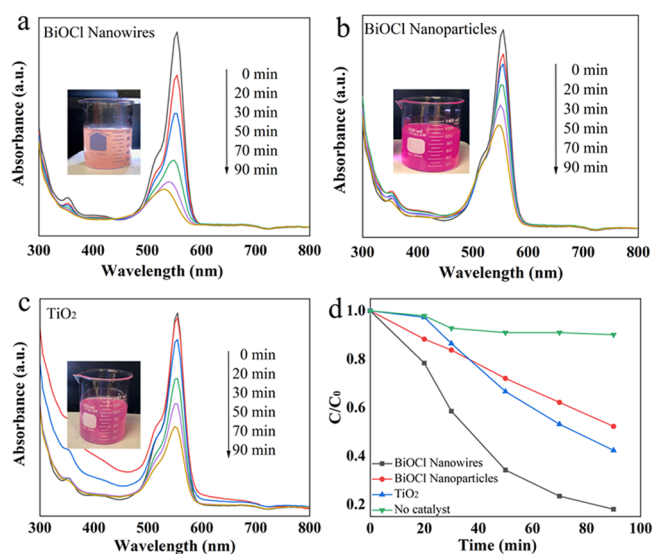


Figure 4. RhB photodecomposition with (a) BiOCl nanowires, (b) commercial BiOCl nanoparticles, and (c) TiO₂ under the simulated solar irradiation. (d) Comparison of photodecomposition of RhB vs time. Photocatalysts (10 mg) were added into 100 mL of 10⁻⁵ M RhB aqueous solution for each case.

nanocluster basis, since the size of nanoclusters continuously decrease during the observation time. A dense network of BiOCl nanowires is formed at 360 min (Figure 4c). With further increasing the stirring time, the growth rate decreases. It is found that lower aspect-ratio nanorods are obtained in the case of 480 and 640 min (Figure S4), likely caused by the decreasing concentration of chloride ions.

To investigate the role of NaCl concentration in the nanowire formation, we check the SEM image of products synthesized using 0.5 M NaCl solution in which a 3D microstructure with nanoflakes instead of nanowires is obtained (Figure S5). It is deduced that the NaCl concentration affects the attachment process of primary nanoflakes. It was widely reported that long-distance electrostatic force serves as the driving force for the OA process.³⁰ In

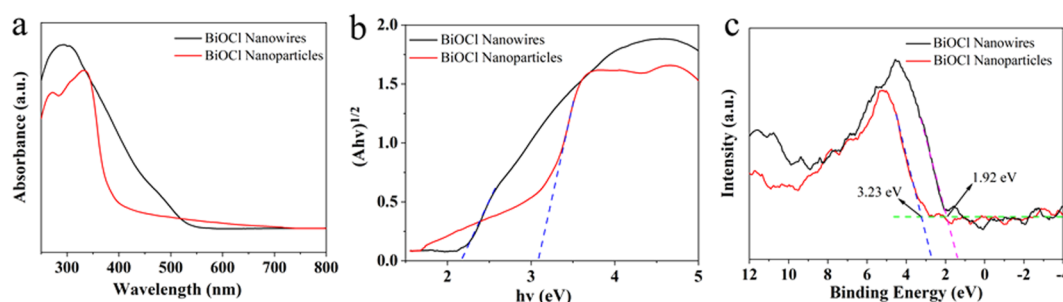


Figure 5. (a) UV–vis diffuse reflectance spectra of the BiOCl nanowires and commercial BiOCl powder; (b) calculated curve of $(Ah\nu)^{1/2}$ versus photon energy is plotted, and the band gaps are estimated from the intersection between the dashed line and horizontal axis; (c) valence-band XPS spectra of BiOCl nanowires and commercial BiOCl powders.

the case of saturated solution, the layered crystal structure of BiOCl results in excessive hydrated chloride ions adsorbed on the {001} facets of primary nanoflakes or nanoclusters, which obstructs further attachment to the {001} facets and allows formation of nanoneedles aligning in the perpendicular direction. In addition to the initial concentration of NaCl, it is worth mentioning that reaction temperature is crucial for the formation of BiOCl nanowires. The low temperature is favorable in the nanowire formation, while only BiOCl particles with a 3D microstructure are obtained with a temperature of 50 and 80 °C (Figure S6). Possibly due to the dependence of ion adsorption on temperature, the orientation attachment of primary particles is affected.

For simplicity, the growth mechanism for BiOCl nanowires can be understood through three steps as depicted in Figure 4d. Initially, BiOCl nanoflakes or nanoclusters are formed via the chemical reaction of Bi_2O_3 with Cl^- ions. While primary particles aggregate around the nanoclusters and subsequently crystallize to a single crystal, the constraint of excessive Cl^- ions adsorbed on the (001) planes of nanoflakes induces the protrusion of nanoneedles along the direction perpendicular to [001] via OA. Finally, the growth of nanowires is accelerated with depleting nanoflakes or nanoclusters, and a network of nanowires is achieved. This growth mechanism can be extended to other bismuth oxyhalides. We obtained BiOBr nanowires with stirring Bi_2O_3 powder in the saturated NaBr solution, where the excessive Br ions dominate the process of nanowire growth. It underpins an efficient strategy for massively synthesizing photocatalytic semiconductors.

2.3. Photocatalytic Activity of BiOCl Nanowires. The photocatalytic activity of BiOCl nanowires was evaluated via the RhB degradation under the simulated irradiation of visible light, while the commercial TiO_2 powders and BiOCl nanoparticles were adopted for controlled experiments. Inappreciable decomposition of RhB in the aqueous solution is observed without photocatalysts, indicating the negligible photolysis for RhB. It is evident that the declining rate of the peak intensity for BiOCl nanowires is significantly higher than that for TiO_2 powder or the commercial BiOCl (Figure 4a–c). The relative concentration C/C_0 of RhB is plotted with the illumination time (Figure 4d). The decoloration rate of RhB for BiOCl nanowires can reach 80% after 90 min, while only 50% of RhB molecules are decomposed with either the TiO_2 powder or BiOCl nanoparticles after 90 min of reaction. The reaction kinetics of photodegradation are quantified by fitting the experimental data to the Langmuir–Hinshelwood model, and we adopt the simplified model of pseudo first-order kinetics, $-\ln(C(t)/C_0) = kt$ with k as the apparent first-order

rate constant, since the reactant concentration is at the millimolar range.¹⁹ The apparent rate constant k is calculated to be 0.39, 0.13, 0.18, and 0.02 min^{-1} for BiOCl nanowires, commercial BiOCl, TiO_2 , and no catalyst, respectively (Figure S8). The RhB decomposition capability of BiOCl nanowires is much higher than that of the other two catalysts or other recently reported BiOCl nanostructures.² Additionally, XRD spectra before and after degradation illustrated that the crystal structure of BiOCl nanowires was maintained (Figure S10). It is also noted that the photoactivity of reactant Bi_2O_3 to degrade RhB is negligible (Figure S11). Therefore, our results evidently demonstrate that the as-synthesized BiOCl nanowires have superior photocatalytic activity under visible light, which is contributed by the structure of high aspect-ratio nanowires and exposed reactive {001} facets.^{19,24,28}

To explore the underlying mechanism for enhanced photocatalytic activity, we further analyzed the band structure feature of BiOCl nanowires. The optical adsorption properties of the as-prepared BiOCl nanowires and commercial BiOCl nanoparticles were studied via UV–vis diffuse reflection spectra (Figure 5a). The adsorption behaviors are in agreement with the color of BiOCl nanowires and commercial BiOCl nanopowders, which are light yellow and white, respectively. According to previous theories, the band gap E_g of the semiconductor is related to the photon energy $h\nu$ via the formula $(\alpha h\nu)^{1/n} = A(h\nu - E_g)$, where α and A are the absorption coefficient and a constant, and n is 2 for the BiOCl semiconductor.²⁸ The Tauc plots ($(Ah\nu)^{1/2}$ vs $h\nu$) of the as-synthesized BiOCl and commercial BiOCl nanoparticles are calculated in Figure 5b. Estimated from the absorption onsets indicated by dashed lines, the band gaps are determined to be approximately 2.3 and 3.2 eV for BiOCl nanowires and BiOCl nanoparticles, respectively. It is indicated that BiOCl nanowires have a narrower band gap, which results in adsorbing more solar energy in the catalytical degradation under visible-light irradiation. The difference in the band gap can be attributed to the predominant exposed {001} facets and the high aspect-ratio structure in BiOCl nanowires.

The valence band position potentials (E_{VB}) of both BiOCl nanowires and commercial BiOCl powder were measured by XPS valence spectra, as shown in Figure 5c. The E_{VB} with a maximum energy edge for BiOCl nanowires is estimated to be $E_{VB}^{\text{max}} = 1.92\text{V}$. According to the band gap, the conduction band minimum locates at $E_{CB}^{\text{min}} = -0.38\text{V}$. Compared to BiOCl nanoparticles, the maximum valence band and the conduction band minimum for BiOCl nanoparticles down-shift by 1.31 and 0.41 eV, respectively. According to the requirement for direct semiconductor photoexcitation in the photocatalytic

reaction, the up-shifting of the conduction band in BiOCl nanowires is beneficial for providing more reductive photoexcited electrons and inhibiting the electron–hole recombination for improved transferring photoexcited electrons to reactants.^{19,24} Furthermore, the photocurrents of BiOCl nanowires and commercial nanoparticles are compared (Figure S12), which exhibited a larger current density for the nanowire. Thus, BiOCl nanowires exhibit better performance in the suppression of the recombination of photogenerated electrons and holes than that for the commercial BiOCl nanoparticles.

3. CONCLUSIONS

To sum up, we have proposed a highly facile synthesis method for growing BiOCl nanowires with stirring Bi₂O₃ powder in the saturated NaCl solution. The mechanism of OA was revealed with primary BiOCl nanoflakes assembled into BiOCl nanowires. With changed electronic structure and highly exposed active (001) facets, the nanowire structure has a narrow band gap. The prepared BiOCl nanowires exhibited a higher photocatalytic activity for decomposing RhB than those by TiO₂ and commercial BiOCl powders under visible-light illumination. The easy synthesis and excellent performances open new insights for massive and economical application of BiOCl nanostructures as the photocatalyst.

4. EXPERIMENTAL SECTION

4.1. Synthesis of BiOCl Nanowires. To prepare the BiOCl nanowires, 0.932 g (2 mmol) of Bi₂O₃ powder was added into 10 mL of the saturated NaCl solution followed by stirring at room for 6 h. The synthesized solid powder was collected by centrifugation and rinsing four times with deionized water and alcohol to remove soluble salts. The final product was dried at 65 °C for 12 h prior to characterization and testing.

4.2. Physicochemical Characterization of BiOCl Nanowires. The crystal structures of BiOCl and Bi₂O₃ were collected using a PANalytical X'Pert³ XRD instrument with high-intensity Cu K α radiation. The morphology of all samples was characterized through a SIGMA VP ZEISS scanning electron microscope. The transmission electron microscopy (TEM) analysis for BiOCl nanowires was conducted by drop-casting a BiOCl ethanol dispersion onto a lacy carbon TEM grid on an FEI Helios NanoLab 660 SEM/FIB system. The TEM specimens were thinned using a 30 kV Ga ion beam and further cleaned with the aid of a 5 kV Ga beam. The chemical composition and valence state of the constituent elements were acquired using a Phi 5500 XPS instrument with an Al X-ray source applied.

4.3. Photocatalytic Degradation of BiOCl Nanowires. The photocatalytic activities of the BiOCl nanowire samples were examined through photodegradation of Rhodamine B (RhB) under simulated solar irradiation from a 150 W Xe lamp ($\lambda = 300\text{--}800$ nm), and the light intensity at the sample was benchmarked to be 7.5 mW/cm² by adjusting the distance between the sample and lamp. BiOCl nanowires (10 mg) as a photocatalyst were added into 100 mL of 10⁻⁵ M RhB aqueous solution. Prior to illumination, the suspension was placed in the dark and stirred for 20 min in order to ensure an adsorption/desorption equilibrium. A suspension (5 mL) was collected every 10 min under visible-light illumination and then centrifuged to remove insoluble catalyst powders. The concentration of RhB was determined by monitoring its characteristic absorption at 554 nm with a UV–vis spectrometer. All measurements were carried out at ambient temperature. To evaluate the photocatalytic activities of BiOCl nanowires, experiments of photocatalytic degradation using the commercial BiOCl and TiO₂ powders were also performed under identical conditions.

■ ASSOCIATED CONTENT

Supporting Information

The Supporting Information is available free of charge at <https://pubs.acs.org/doi/10.1021/acsanm.1c00288>.

Characterization of BiOCl samples and quantified reaction kinetics of photo-degradation (PDF)

■ AUTHOR INFORMATION

Corresponding Authors

Yuan Yang – Program of Materials Science and Engineering, Department of Applied Physics and Applied Mathematics, Columbia University, New York, New York 10027, United States; orcid.org/0000-0003-0264-2640; Email: yy2664@columbia.edu

Xi Chen – Earth Engineering Center; Center for Advanced Materials for Energy and Environment, Department of Earth and Environmental Engineering, Columbia University, New York, New York 10027, United States; orcid.org/0000-0002-8911-4172; Email: xichen@columbia.edu

Authors

Xiangbiao Liao – Earth Engineering Center; Center for Advanced Materials for Energy and Environment, Department of Earth and Environmental Engineering, Columbia University, New York, New York 10027, United States; orcid.org/0000-0001-8214-454X

Xin Lan – Earth Engineering Center; Center for Advanced Materials for Energy and Environment, Department of Earth and Environmental Engineering, Columbia University, New York, New York 10027, United States

Nan Ni – Program of Materials Science and Engineering, Department of Applied Physics and Applied Mathematics, Columbia University, New York, New York 10027, United States

Pengfei Yang – Earth Engineering Center; Center for Advanced Materials for Energy and Environment, Department of Earth and Environmental Engineering, Columbia University, New York, New York 10027, United States; School of Mechanical Engineering and Automation, Fuzhou University, Fuzhou 350108, China

Complete contact information is available at: <https://pubs.acs.org/doi/10.1021/acsanm.1c00288>

Author Contributions

^{||}X.L., X.L. and N.N. contributed equally to this work.

Author Contributions

X.B.L., N.N. and X.L. performed the catalyst preparation and wrote this paper. X.B.L. and Y.P.F. performed characterization tests. X.B.L. and X.L. performed performance tests and data analysis. X.B.L., N.N., Y.Y., and X.C. designed the study. All authors discussed the results and commented on the manuscript.

Notes

The authors declare no competing financial interest.

■ ACKNOWLEDGMENTS

The work of X.B.L. and X.C. was supported by Earth Engineering Center and Center for Advanced Materials for Energy and Environment. The Xe lamp and UV–vis spectrometer are offered by Prof. Daniel Esposito's research group from Columbia Engineering.

■ REFERENCES

- (1) Honda, K. Electrochemical Photolysis of Water at a Semiconductor Electrode. *Nature* **1972**, *238*, 37–38.
- (2) Cheng, H.; Huang, B.; Dai, Y. Engineering BiOX (X = Cl, Br, I) nanostructures for highly efficient photocatalytic applications. *Nanoscale* **2014**, *6*, 2009–2026.
- (3) Serpone, N.; Emeline, A. V. Semiconductor Photocatalysis — Past, Present, and Future Outlook. *J. Phys. Chem. Lett.* **2012**, *3*, 673–677.
- (4) Arthur, R.; Ahern, J.; Patterson, H. Application of BiOX Photocatalysts in Remediation of Persistent Organic Pollutants. *Catalysts* **2018**, *8*, 604.
- (5) Ni, M.; Leung, M. K. H.; Leung, D. Y. C.; Sumathy, K. A review and recent developments in photocatalytic water-splitting using TiO₂ for hydrogen production. *Renew. Sust. Energ. Rev.* **2007**, *11*, 401–425.
- (6) Zhang, Y.; Lv, F.; Wu, T.; Yu, L.; Zhang, R.; Shen, B.; Meng, X.; Ye, Z.; Chu, P. K. F and Fe co-doped TiO₂ with enhanced visible light photocatalytic activity. *J. Sol-Gel Sci. Technol.* **2011**, *59*, 387–391.
- (7) Choi, W. Visible light active platinum-ion-doped TiO₂ photocatalyst. *J. Phys. Chem. B* **2005**, *109*, 24260.
- (8) Gao, Z.; Chen, K.; Wang, L.; Bai, B.; Liu, H.; Wang, Q. Aminated flower-like ZnIn₂S₄ coupled with benzoic acid modified g-C₃N₄ nanosheets via covalent bonds for ameliorated photocatalytic hydrogen generation. *Appl. Catal., B* **2020**, *268*, 118462.
- (9) Jin, P.; Wang, L.; Ma, X.; Lian, R.; Huang, J.; She, H.; Zhang, M.; Wang, Q. Construction of hierarchical ZnIn₂S₄@ PCN-224 heterojunction for boosting photocatalytic performance in hydrogen production and degradation of tetracycline hydrochloride. *Appl. Catal., B* **2021**, *284*, 119762.
- (10) Li, J.; Li, H.; Zhan, G.; Zhang, L. Solar Water Splitting and Nitrogen Fixation with Layered Bismuth Oxyhalides. *Acc. Chem. Res.* **2017**, *50*, 112–121.
- (11) Li, J.; Yu, Y.; Zhang, L. Bismuth oxyhalide nanomaterials: layered structures meet photocatalysis. *Nanoscale* **2014**, *6*, 8473–8488.
- (12) Zhang, X.; Liu, X.; Fan, C.; Wang, Y.; Wang, Y.; Liang, Z. A novel BiOCl thin film prepared by electrochemical method and its application in photocatalysis. *Appl. Catal., B* **2013**, *132–133*, 332–341.
- (13) Li, H.; Shang, J.; Zhu, H.; Yang, Z.; Ai, Z.; Zhang, L. Oxygen Vacancy Structure Associated Photocatalytic Water Oxidation of BiOCl. *ACS Catal.* **2016**, *6*, 8276–8285.
- (14) Chen, F.; Liu, H.; Bagwasi, S.; Shen, X.; Zhang, J. Photocatalytic study of BiOCl for degradation of organic pollutants under UV irradiation. *J. Photochem. Photobiol., A* **2010**, *215*, 76–80.
- (15) Ma, X.; Chen, K.; Niu, B.; Li, Y.; Wang, L.; Huang, J.; She, H.; Wang, Q. Preparation of BiOCl_{0.9}IO_{0.1}/β-Bi₂O₃ composite for degradation of tetracycline hydrochloride under simulated sunlight. *Chin. J. Catal.* **2020**, *41*, 1535–1543.
- (16) Burford, N. Bismuth Compounds and Preparations with Biological or Medicinal Relevance. *Chem. Rev.* **1999**, *99*, 2601–2658.
- (17) Li, D. Highly efficient Bi₂O₂CO₃/BiOCl photocatalyst based on heterojunction with enhanced dye-sensitization under visible light. *Appl. Catal. B Environ.* **2016**, *187*, 301–309.
- (18) Fan, W.; Li, C.; Bai, H.; Zhao, Y.; Luo, B.; Li, Y.; Ge, Y.; Shi, W.; Li, H. An in situ photoelectroreduction approach to fabricate Bi/BiOCl heterostructure photocathodes: understanding the role of Bi metal for solar water splitting. *J. Mater. Chem. A* **2017**, *5*, 4894–4903.
- (19) Guan, M.; Xiao, C.; Zhang, J.; Fan, S.; An, R.; Cheng, Q.; Xie, J.; Zhou, M.; Ye, B.; Xie, Y. Vacancy associates promoting solar-driven photocatalytic activity of ultrathin bismuth oxychloride nanosheets. *J. Am. Chem. Soc.* **2013**, *135*, 10411–10417.
- (20) Cao, S.; Guo, C.; Lv, Y.; Guo, Y.; Liu, Q. A novel BiOCl film with flowerlike hierarchical structures and its optical properties. *Nanotechnology* **2009**, *20*, 275702.
- (21) Xiong, J.; Cheng, G.; Qin, F.; Wang, R.; Sun, H.; Chen, R. Tunable BiOCl hierarchical nanostructures for high-efficient photocatalysis under visible light irradiation. *Chem. Eng. J.* **2013**, *220*, 228–236.
- (22) Tian, Y.; Guo, C. F.; Guo, Y.; Wang, Q.; Liu, Q. BiOCl nanowire with hierarchical structure and its Raman features. *Appl. Surf. Sci.* **2012**, *258*, 1949–1954.
- (23) Wu, S.; Wang, C.; Cui, Y.; Wang, T.; Huang, B.; Zhang, X.; Qin, X.; Brault, P. Synthesis and photocatalytic properties of BiOCl nanowire arrays. *Mater. Lett.* **2010**, *64*, 115–118.
- (24) Zhang, X.; Wang, X. B.; Wang, L. W.; Wang, W. K.; Long, L. L.; Li, W. W.; Yu, H. Q. Synthesis of a highly efficient BiOCl single-crystal nanodisk photocatalyst with exposing {001} facets. *ACS Appl. Mater. Interfaces* **2014**, *6*, 7766–7772.
- (25) Lieber, C. M. Diameter-controlled synthesis of single-crystal silicon nanowires. *Appl. Phys. Lett.* **2001**, *78*, 2214–2216.
- (26) Lieber, C. M. General Synthesis of Compound Semiconductor Nanowires. *Adv. Mater.* **2010**, *12*, 298–302.
- (27) Li, G.; Jiang, B.; Xiao, S.; Lian, Z.; Zhang, D.; Yu, J. C.; Li, H. An efficient dye-sensitized BiOCl photocatalyst for air and water purification under visible light irradiation. *Environ. Sci. Process Impacts* **2014**, *16*, 1975–1980.
- (28) Wang, C. Y.; Zhang, X.; Song, X. N.; Wang, W. K.; Yu, H. Q. Novel Bi(1)(2)O(1)(5)Cl(6) Photocatalyst for the Degradation of Bisphenol A under Visible-Light Irradiation. *ACS Appl. Mater. Interfaces* **2016**, *8*, 5320–5326.
- (29) Pu, F.; Lu, X.; Xia, Y.; Huang, W.; Li, Z. Preparation of Surface-Sulfurized Nanoflake-Like BiOCl Layered Semiconductor Films with Interbedded S₂—for Enhanced Photoelectrochemical Performances. *J. Electrochem. Soc.* **2014**, *161*, H269–H275.
- (30) Yella, A.; Gautam, U. K.; Mugnaioli, E.; Panthöfer, M.; Bando, Y.; Golberg, D.; Kolbc, U.; Tremel, O. Asymmetric tungsten oxide nanobrushes via oriented attachment and Ostwald ripening. *CrystEngComm* **2011**, *13*, 4074–4081.
- (31) Gao, L. Growth of Well-Defined Cubic Hematite Single Crystals: Oriented Aggregation and Ostwald Ripening. *Cryst. Growth Des.* **2008**, *8*, 1372–1376.